Water depth dependence of long-range correlation in nontidal variations in seafloor pressure

Tomohiro Inoue[1], Yoshihiro Ito[2], Laura M. Wallace[3,4], Yutaka Yoshikawa[1], Daisuke Inazu[5], Emmanuel Soliman Mortel Garcia[2], Tomoya Muramoto[6], Kazuaki Ohta[7], Syuichi Suzuki[8], Ryota Hino[8], Spahr C. Webb[9]

[1] Graduate School of Science, Kyoto University, Kyoto, Japan

[2] Disaster Prevention Research Institute, Kyoto University, Uji, Japan

[3]GNS Science, Lower Hutt, New Zealand

[4]Institute for Geophysics, University of Texas at Austin, Austin, TX, USA

[5]Department of Marine Resource and Energy, Tokyo University of Marine Science and Technology, Tokyo, Japan

[6]National Metrology Institute of Japan, National Institute of Advanced Industrial Science and Technology, Tsukuba, Japan

[7]National Research Institute for Earth Science and Disaster Resilience, Tsukuba, Japan

[8]Graduate School of Science, Tohoku University, Sendai, Japan

[9]Lamont-Doherty Earth Observatory, Columbia University, Palisades, NY, USA

Corresponding author: Tomohiro Inoue (inoue.tomohiro.48n@st.kyoto-u.ac.jp)

Key Points:

- The similarity of the non-tidal components of bottom pressure varies with relative water depth, rather than distance between sites.
- Bottom pressure data show that reference sites at similar depths will optimize oceanographic noise removal for seafloor geodetic studies.
- Oceanographic models with baroclinicity reproduce the depth dependence of the nontidal variations better than barotropic models.

Abstract

Isolating the source of non-tidal oceanographic noise in seafloor pressure data is critical for improving the use of these data for seafloor geodetic applications. Residuals between nearby bottom pressure records have typically been used to remove the non-tidal components, as these are largely common-mode. To evaluate the similarities between pairs of observed bottom pressure records at a range of water depths, we calculate the standard deviations of the time series of residuals between data from all site pairs, recorded during a recent experiment offshore New Zealand. Similar to a recent study offshore Cascadia, we find that the magnitude of the standard deviation depends more on relative water depth than the distance between sites. This confirms that non-tidal components are more similar along isobaths even if the distance between sites is large. We show that the depth range varies with the depth of the deeper site of the pairs under restrictions.

Plain Language Summary

Coherent signals of ocean bottom pressure are observed along common water depths within an ocean bottom pressure array offshore New Zealand. We statistically evaluated the similarity of the seafloor pressure collected in 2014 offshore the North Island's east coast, where the Pacific Plate dives or "subducts" along the Hikurangi subduction zone beneath the North Island. This is important for removal of noise caused by oceanographic processes, which must be done to detect centimeter-level vertical movement of the seafloor crust during slow slip events using seafloor pressure records. We measured the similarity of pairs of seafloor pressure records at a range of water depths. Similar to a recent study offshore the Cascadia subduction zone, our results confirm that seafloor pressure records from similar depths (but at large horizontal distances from each other) can be used effectively to reduce oceanographic noise in sea floor pressure data to reveal the seafloor crustal deformation.

1. Introduction

Temporal fluctuations in ocean bottom pressure originate from phenomena at varying spatio-temporal scales over the Earth's surface driven by atmospheric and oceanic circulation, tides, tsunamis, and tectonic deformation of the crust. Ocean-bottom pressure gauges (OBPs) are becoming widely used to measure tectonic signals, particularly those caused by tectonic deformation in some subduction zones (e.g., Menemenlis et al., 2008 (ECCO2); Inazu et al., 2012 (IN12); Ito et al., 2011, 2013; Hino et al., 2014; Davis et al., 2015; Suzuki et al., 2016; Wallace et al., 2016; Sato et al., 2017; Muramoto et al., 2019; Fredrickson et al., 2019). Previous studies have used OBPs to record vertical seafloor deformation during episodic slow slip events (SSEs), enabling the investigation of SSE-related deformation characteristics near the trench axis (e.g., Ito et al., 2013; Davis et al., 2015; Wallace et al., 2016).

SSEs are common to many subduction zones (e.g., Hirose et al., 1999; Heki & Kataoka, 2008; Wallace & Beavan, 2010; Nishimura et al., 2013; Ozawa, 2014). It is difficult to characterize SSEs beneath the seafloor using land-based global navigation satellite system (GNSS) networks, due to the lack of ability of onshore networks to resolve deformation occurring on offshore faults. The advantage of OBPs is that the seafloor crustal deformation associated with transient deformation, such as SSEs, can be continuously recorded with a

resolution of 1-3 centimeters (e.g., Ito et al., 2011; Davis et al., 2015; Suzuki et al., 2016; Wallace et al., 2016; Fredrickson et al., 2019).

The greatest challenge associated with using OBPs for seafloor geodetic investigations to detect cm-level vertical crustal deformation is the presence of oceanographic noise in seafloor pressure data, which can be on the order of 1–2 meters for the tidal components, and tens of centimeters for non-tidal components. To remove the oceanographic noise, two approaches are commonly used: (1) oceanographic modeling to estimate and remove the non-tidal component (Hino et al., 2014; Sato et al., 2017; Muramoto et al., 2019), and (2) a reference-station method using pressure records from a reference station outside of the deforming zone to remove the oceanographic noise under the assumption that the non-tidal components are common-mode over a large region (Ito et al., 2013; Davis et al., 2015; Wallace et al., 2016; Frederickson et al., 2019).

The oceanographic modeling approach to reducing oceanographic noise in OBP data is undertaken by subtracting the seafloor pressure predicted by the ocean model from the observed pressure (e.g., Hino et al., 2014; Sato et al., 2017; Muramoto et al., 2019). Various modeling approaches have been developed to calculate nontidal oceanographic variations, including a global baroclinic ocean model using assimilated wind vector and heat flux (e.g., ECCO2), and global barotropic ocean models driven by assimilated wind vectors and the sea surface pressures (IN12) published by the 55-year Japanese Reanalysis Project (Kobayashi et al., 2015; Harada et al., 2016). By applying the barotropic model, Hino et al. (2014) suppressed oceanographic noise and detected crustal deformation (less than 5cm) associated with afterslip of the largest foreshock following the 2011 Mw 9.0 Tohoku-Oki earthquake. At the Hikurangi subduction zone, the variance reduction using the oceanographic models (~60%) was significantly less than that obtained using reference sites for noise removal (~80-90%) (Muramoto et al., 2019), suggesting that when suitable reference sites are available, the reference site approach is generally more robust.

In the reference-station method, subtraction of the pressure data from the reference site OBPs is commonly used assuming that the effects of oceanographic variability are largely common-mode across the network footprint (e.g., Ito et al., 2013; Wallace et al., 2016). Adjacent to the hypocenter of the 2011 Mw 9.0 Tohoku-Oki earthquake, crustal deformation of a few centimeters due to slow slip was detected as relative vertical displacement, which was inferred from pressure differences among several OBP pairs before the 2011 Tohoku-Oki earthquake (Ito et al., 2013). At the northern Hikurangi subduction zone offshore the North Island of New Zealand, Wallace et al. (2016) observed 1–5 cm of vertical crustal deformation during a September/October 2014 SSE using OBP data (which was also observed by onshore GNSS stations), and concluded that the slip may have reached the vicinity of the trench axis. Fredrickson et al. (2019) recently demonstrated coherence in bottom pressure changes observed between sites in similar water depths offshore Cascadia, leading them to propose a new method of placing reference sites at common isobaths to achieve large reductions in oceanographic noise in OBP time series. Here, we further evaluate the efficiency of considering differences between bottom pressure pairs at a range of water depths using the OBP data acquired during a 2014–2015 experiment offshore New Zealand.

2. Seafloor pressure data

We use data from OBPs deployed from mid-2014 to mid-2015 (Fig. 1) along the east coast of the North Island of New Zealand. These data originate from the Hikurangi Ocean Bottom Investigation of Tremor and Slow Slip (HOBITSS) experiment, which deployed 24 autonomous OBPs and 15 ocean-bottom seismometers (OBS) aimed at investigating offshore SSEs and their relationship to tectonic tremor and earthquakes along the Hikurangi trough (e.g., Wallace et al., 2016; Todd et al., 2018; Warren-Smith et al., 2019; Yarce et al., 2019; Yohler et al., 2019; Zal et al., 2020). The instruments in these dense arrays were deployed directly above the source region of shallow (< 10 km depth) slow slip events at the north Hikurangi margin (Wallace et al., 2016).

In general, pressure changes recorded by an OBP are described as a pressure $\boldsymbol{P_{ref}}$ corresponding to the water depth and a pressure deviation $\boldsymbol{\Delta P_B(t)}$ that fluctuates around the pressure $\boldsymbol{P_{ref}}$ (Eq. (1)). A linear relationship between various components, including the crustal deformation component $\boldsymbol{\Delta P_C(t)}$ (e.g., IN12), represents the seafloor pressure fluctuation $\boldsymbol{\Delta P_B(t)}$ (Eq. (2)), as follows:

$$\boldsymbol{P_B(t) = P_{ref} + \Delta P_B(t)} \tag{1}$$

$$\boldsymbol{\Delta P_B(t) = \Delta P_C(t) + \Delta P_T(t) + \Delta P_O(t) + \Delta P_D(t) + \varepsilon(t)} \tag{2}$$

where, $\boldsymbol{\Delta P_C(t)}$ is the pressure change due to the vertical seafloor deformation, $\boldsymbol{\Delta P_T(t)}$ is the pressure change due to the ocean tide and the Earth tides (mainly diurnal and semi-diurnal tides; ~ 100 hPa (Ray, 2013)), $\boldsymbol{\Delta P_O(t)}$ is the pressure change due to nontidal oceanic variations such as ocean currents, eddies, and sea surface pressure changes (Ponte & Ray, 2002; ECCO2; IN12; Cummings & Smedstad, 2013), $\boldsymbol{\Delta P_D(t)}$ is the pressure changes due to instrument drift (e.g. Kajikawa & Kobata, 2019), and $\boldsymbol{\varepsilon(t)}$ is the unmodeled noise.

3. Coherent signals on bottom pressure between sites

We adopted two statistical quantities to evaluate the similarity between all pairs of OBP data in the HOBITSS experiment: (i) standard deviation (SD, Eq. (3)) of the residual pressure between a pair of sites and (ii) correlation coefficient (CC, Eq. (4)) between a pair of sites. After removing the tidal components and instrument drift from the observed data, we calculated both the SD and CC. Using the SD, CC, the depth and distance dependence of the pressure signals were evaluated within the HOBITSS OBP array (Table S1). The tides were removed by applying a low pass filter (cut off period: 2 days). Instrumental drift was estimated and removed by fitting an exponential and a linear term (see Fig. S1 for details) (Polster et al., 2009). The SD and CC equations are expressed as follows:

$$\boldsymbol{SD = \sqrt{\frac{1}{N}\sum_{1}^{N}(P_t^{i,j} - A^{ij})^2}} \tag{3}$$

$$\boldsymbol{CC = \frac{\sum_1^N (P_t^i - A^i)(P_t^j - A^j)}{\sqrt{\sum_1^N (P_t^i - A^i)^2}\sqrt{\sum_1^N (P_t^j - A^j)^2}}} \tag{4}$$

where P_t^i and P_t^j denote the pressure anomaly at the time t at stations i and j, respectively. A^i and A^j denote the average of the time series of P_t^i and P_t^j, respectively. $P_t^{i,j}$ is the result of P_t^i minus P_t^j. A^{ij} is the average of the time series of the residual pressure ($P_t^{i,j}$), and N is the number of data in the time series.

4. Relative water depth dependence on bottom pressure along an isobath

We analyzed two time windows (185–265 days and 285–350 days from Jan. 1 2014), which did not include the two SSE periods in September/October 2014 (Wallace et al., 2016) and late December 2014 that were observed on nearby continuous GNSS data (Fig. S2). The OBP records after the second SSE were not analyzed due to a lack of data at some sites which stopped recording later in the experiment. We show example time series from pairs of OBP sites from days 185–265 at similar distances apart (~30 km) for 3 cases: (i) a large depth difference (1674 m), (ii) an intermediate depth difference (579 m), and (iii) from sites at similar depth (depth difference: 114 m) (Fig. 2).

Non-tidal components observed on the OBPs in the HOBITSS network show strong similarities between site pairs at similar water depths (e.g., within 500–1000 m of each other). The similarity decreases with increasing relative depths between the sites (185–265 days in Figs. 3a–3e, 285–350 days in Fig. S2a). In contrast, there appears to be very little dependence of the SD on the horizontal distance between site pairs (maximum distance between sites ~75 km), as no significant increase in the SD as a function of the inter-site distance was observed (185–265 days in Fig. 3f–3j, 285–350 days in Fig. S3). An R value of 0.57 was calculated for the correlation between the SD of pair-wise residual pressure versus the relative depth difference (Fig. 3a), compared with a value of 0.17 for the correlation of the residual pressure versus the inter-site distance (Fig. 3f). The correlations depended on the depths of the sites. In addition, the R values were calculated for the scatter plot of the SD against the depth of the deeper site in each pair, with results of 0.45, 0.86, 0.86, and 0.81 for depth ranges of less than 1300 m, 1300–2000 m, 2000–2500 m, and more than 2500 m, respectively. This suggests that the bottom pressure data from site pairs deeper than 1300 m are much more strongly correlated, and that larger depth seaparations between such site pairs may be suitable for enhanced oceanographic noise removal. Similarly, the R value of -0.52 is calculated from the scatter distribution of CC as a function of relative water depth difference (185–265 days in Figs. S4a–S4e, 285–350 days in Figs. S5a). In contrast, an R value of -0.13 is calculated as a function of inter-site distance (185–265 days in Figs. S4f–S4j, 285–350 days in Fig. S5b). The CC shows a strong dependence on depth difference (185–265 days in Fig. S4, 285–350 days in Fig. S5), further indicating that the similarity in nontidal components observed in ocean bottom pressure depends on relative water depth, but not on relative distance.

The pair-wise SDs calculated from the HOBITSS data were grouped according to whether the values fall under a certain threshold (less than 0.5, 1.0, and 1.5 hPa), and these were found to vary widely depending on the depth of the deeper site of the site pairs (Figs. 3, 4). The SDs from the shallower pairs where the deeper site is located at less than 2500 m rapidly increase with increasing depth difference, suggesting that for sites in < 2500 m water depth, reference sites within 500-1000 m water depth of other sites are needed to reduce the oceanographic noise levels to below 1–1.5 hPa, and a depth difference of < 250 m is required to reduce this to < 0.5 hPa (e.g., Figs. 3b–3d, 4a). In contrast, the SDs from the pairs with the deeper depths (> 2500 m) increase more gradually–remaining < 1 hPa even with the depth

differences of 2200 m (Figs. 3e, 4a). This suggests that for deeper sites (e.g., located at depths > 2500 m), reference sites from a broader range of depths can be utilized.

Viewing the results in terms of a normalized water depth range, calculated by dividing the depth range by the depth of deepest site (of the pair) (Fig. 4), is also a useful guide for reference site selection. To achieve SDs < 1hPa, for instance, the depth range of the pair must be within a normalized depth of approximately 0.5, or less than half the depth of the deepest site (Fig. 4b). However, for the deep site LOBS4 (3441 m depth), SDs less than 1.0 and 1.5 hPa are calculated for reference sites that are 2194 m and 2451 m shallower than LOBS4 (Fig. 4a). For SBPR2 (2116 m depth), SDs less than 0.5, 1.0 and 1.5 hPa are calculated using sites that are 243 m, 672 m and 1127 m shallower than SBPR2, respectively (Fig. 4a). For LOBS9 (1457 m depth), SDs less than 0.5, 1.0 and 1.5 hPa are calculated using sites at 211 m, 469 m and 806 m shallower than LOBS9, respectively. This suggests that site pairs with depth differences < 250 m are required if the very low noise levels (e.g., < 0.5 hPa, or < 5 mm) are desired (Fig. 4a). Overall, in the region of HOBITSS experiment, normalized depth ranges of 0.2, 0.5 and 0.7 are required when targeting SDs less than 0.5, 1.0 and 1.5, respectively (Fig. 4b). These characteristics of the HOBITSS OBP data provide a useful indicator for network design strategies which aim for the detection of cm-level crustal deformation from SSEs, and to help guide the design of future OBP networks in New Zealand, and at similar settings.

We also evaluate the water depth dependence of non-tidal components predicted by oceanographic models at the OBP sites using both the baroclinic (ECCO2) and barotropic (IN12) models. The baroclinic ECCO2 model shows similar relative water depth dependence for the predicted differences in ocean bottom pressure records to those in the observed data (Figs. 3a and S6a). In contrast, the dependence on the relative water depth is not significant in the barotropic model (Figs. 3a and S6c). Neither model produces a relative distance dependence, similar to the observed pressure data (Figs. S6b and S6d). The higher R value in the ECCO2 (0.71) relative to IN12 (0.36) indicates that much of the non-tidal component in the observed pressure may originate from baroclinic effects. This result suggests that the baroclinic model reproduces the dependence on relative water depth of actual nontidal components better than the barotropic models. Furthermore, it hints that in terms of the depth dependence of the nontidal variations, the baroclinic models are required if oceanographic models are to be used to correct nontidal effects in OBP data.

Taking the difference between pairs of data at similar water depths can reduce oceanographic noise in the pressure data to less than 1 hPa, which corresponds to 1 cm in terms of the relative vertical deformation (Figs. 3, 4). Previous estimates of seafloor vertical deformation use reference sites seaward of the trench (TXBPR1 and LOBS4; ~3500 m deep) and shows a minimum standard deviation of 0.52 hPa at the deepest site SBPR1 (2453 m deep; Wallace et al., 2016). Previously estimated standard deviations were 1.53 and 1.41 hPa at the sites shallower than 1000 m (TXBPR2 and LOBS8, respectively) when using reference sites on the incoming plate (Muramoto et al., 2019). Using an ocean model (WCOFS - Kurapov et al., 2017) to simulate seafloor pressure records, residuals in Cascadia were estimated to be less than 1 hPa RMS (e.g., < 1 cm) when taking the difference between model sites at similar depths whose range vary with depth (e.g., within 1000m for sites on the abyssal plain) even for sites spaced far apart (< 326 km) (Fredrickson et al., 2019). Those results are comparable to what we observe at the Hikurangi subduction zone. In an OBP network with a higher density of sites, such as the HOBITSS array (which has a maximum site spacing of ~75 km), we clearly demonstrate

that the observed nontidal components have a similarly strong relative water depth dependence, even for the case of a much smaller site spacing such as ours. This reinforces the idea proposed by Frederickson et al. (2019) that the most effective way of utilizing reference sites is to have these sites in similar water depths as the other sites in the areas of interest which are above the zones of deformation, also holds for networks that are relatively dense. For example, for a network, such as HOBITSS, which targets SSEs in a particular area, reference sites along-strike of the SSE region, but at similar water depths to the sites above the SSE area, are the most effective at the removal of oceanographic noise.

5. Conclusions

Using data from a 2014/2015 OBP experiment offshore New Zealand, we showed that the non-tidal components of seafloor pressure are similar along isobaths in the Hikurangi subduction zone. When using the full range of reference site pairs, we found that the standard deviation values for the residual pressure between the site pairs depends strongly on the difference in the depths of the site pairs. The dependence of standard deviation on the water depth difference between the pairs is strong (R=0.57), confirming the previous suggestion of Frederickson et al. (2019) that strong similarities in nontidal oceanographic signals exist between sites at comparable water depths, and that this characteristic can be used to optimize OBP network design for seafloor geodetic investigations. We also found that the similarities of bottom pressure signals have little dependence on the distances between site pairs. To reduce noise levels to below 1 hPa in 2500 m of water depth or less, the water depth difference between site pairs must be < 1000 m. At water depths greater than 2500 m, the oceanographic similarities are greater over larger depth ranges, suggesting that in these cases, reference sites within 2200 m water depth of each other may be suitable for oceanographic noise removal, if targeting < 1 hPa residual noise levels. If targeting even lower noise levels, smaller depth differences between reference sites and the rest of the network will be needed. The simulated non-tidal component of the pressure residuals at the sites as calculated from a baroclinic oceanographic circulation model also showed a strong dependence on depth, as compared with the dependence on the distance. In contrast, barotropic models are unable to reproduce the depth-dependent similarities in non-tidal oceanographic variations, suggesting that in terms of the depth dependence of the nontidal variations, baroclinic models produce a more accurate representation of nontidal signals observed on bottom pressure records. Similar to previous studies in Cascadia, our results highlight the need to consider the placement of reference sites when designing OBP networks with the intent of capturing cm-level transient deformation events, which can be achieved by installing those reference sites at water depths similar to other sites in the rest of the network.

Acknowledgments

This research was supported by the Japan Society for the Promotion of Science KAKENHI program [grant no. 26257206] for Y.I. and the Japan Science and the Technology Agency–Japan International Cooperation Science and Technology Research Partnership for Sustainable Development [grant no. JPMJSA1510], and an NZ MBIE Endeavour fund grant, and NSF grants. We thank the captain and crew of the R/V Tangaroa and the R/V Revelle for deployment and recovery of ocean bottom pressure recorders. The deployment was supported by the NSF grants to Wallace and Webb (OCE- 1334654 and OCE-1333311). Support for ship time came

from NSF, GNS Science, and the New Zealand government-funded Oceans 2020 program. The authors declare that there are no conflicts of interest. The Generic Mapping Tools software v. 5.3.1 (Wessel et al., 2013) was used to prepare the figures. Data are available from the server managed by the authors upon request as well as on the IRIS website (https://www.iris.edu/hq/).

References

Cummings, J. A., & Smedstad, O. M. (2013). Variational Data Assimilation for the Global Ocean. *Data Assimilation for Atmospheric, Oceanic and Hydrologic Applications, II*, 303–343. https://doi.org/10.1007/978-3-642-35088-7

Davis, E. E., Villinger, H., & Sun, T. (2015). Slow and delayed deformation and uplift of the outermost subduction prism following ETS and seismogenic slip events beneath Nicoya Peninsula, Costa Rica. *Earth and Planetary Science Letters*, *410*, 117–127. https://doi.org/10.1016/j.epsl.2014.11.015

Fredrickson, E. K., Wilcock, W. S. D., Schmidt, D. A., MacCready, P., Roland, E., Kurapov, A. L., et al. (2019). Optimizing Sensor Configurations for the Detection of Slow-Slip Earthquakes in Seafloor Pressure Records, Using the Cascadia Subduction Zone as a Case Study. *Journal of Geophysical Research: Solid Earth*. https://doi.org/10.1029/2019JB018053

Harada, Y., Kamahori, H., Kobayashi, C., Endo, H., Kobayashi, S., Ota, Y., et al. (2016). The JRA-55 reanalysis: Representation of atmospheric circulation and climate variability. *Journal of the Meteorological Society of Japan*, *94*(3), 269–302. https://doi.org/10.2151/jmsj.2016-015

Heki, K., & Kataoka, T. (2008). On the biannually repeating slow-slip events at the Ryukyu Trench, southwestern Japan. *Journal of Geophysical Research: Solid Earth*, *113*(11), 1–12. https://doi.org/10.1029/2008JB005739

Hino, R., Inazu, D., Ohta, Y., Ito, Y., Suzuki, S., Iinuma, T., et al. (2014). Was the 2011 Tohoku-Oki earthquake preceded by aseismic preslip? Examination of seafloor vertical deformation data near the epicenter. *Marine Geophysical Research*, *35*(3), 181–190. https://doi.org/10.1007/s11001-013-9208-2

Hirose, H., Hirahara, K., Kimata, F., Fujii, N., & Miyazaki, S. (1999). A slow thrust slip event following the two 1996 Hyuganada earthquakes beneath the Bungo Channel, southwest Japan. *Geophysical Research Letters*, *26*(21), 3237–3240. https://doi.org/10.1029/1999GL010999

Inazu, D., Hino, R., & Fujimoto, H. (2012). A global barotropic ocean model driven by synoptic atmospheric disturbances for detecting seafloor vertical displacements from in situ ocean bottom pressure measurements. *Marine Geophysical Research*, *33*(2), 127–148. https://doi.org/10.1007/s11001-012-9151-7

Ito, Y., Tsuji, T., Osada, Y., Kido, M., Inazu, D., Hayashi, Y., et al. (2011). Frontal wedge deformation near the source region of the 2011 Tohoku-Oki earthquake. *Geophysical Research Letters*, *38*(15), 1–5. https://doi.org/10.1029/2011GL048355

Ito, Y., Hino, R., Kido, M., Fujimoto, H., Osada, Y., Inazu, D., & Ashi, J. (2013). Episodic slow slip events in the Japan subduction zone before the 2011 Tohoku-Oki earthquake. *Tectonophysics*, (600), 14–26. Retrieved from http://dx.doi.org/10.1016/j.tecto.2012.08.022

Kajikawa, H., & Kobata, T. (2019). Evaluation and correction for long-term drift of hydraulic pressure gauges monitoring stable and constant pressures. *Measurement: Journal of the*

International Measurement Confederation, *134*, 33–39. https://doi.org/10.1016/j.measurement.2018.10.051

Kobayashi, S., Ota, Y., Harada, Y., Ebita, A., Moriya, M., Onoda, H., et al. (2015). The JRA-55 reanalysis: General specifications and basic characteristics. *Journal of the Meteorological Society of Japan*, *93*(1), 5–48. https://doi.org/10.2151/jmsj.2015-001

Kurapov, A. L., Erofeeva, S. Y., & Myers, E. (2017). Coastal sea level variability in the US West Coast Ocean Forecast System (WCOFS). *Ocean Dynamics*, *67*(1), 23–36. https://doi.org/10.1007/s10236-016-1013-4

Menemenlis, D., Campin, J.-M., Heimbach, P., Hill, C. N., Lee, T., Nguyen, A. T., et al. (2008). ECCO2: High resolution global ocean and sea ice data synthesis. *Mercator Ocean Quarterly Newsletter*, *31*(October), 13–21. Retrieved from http://www.mercator-ocean.fr/content/download/691/5904/version/1/file/lettre_31_en.pdf#page=13

Muramoto, T., Ito, Y., Inazu, D., Wallace, L. M., Hino, R., Suzuki, S., et al. (2019). Seafloor Crustal Deformation on Ocean Bottom Pressure Records With Nontidal Variability Corrections: Application to Hikurangi Margin, New Zealand. *Geophysical Research Letters*, *46*(1), 303–310. https://doi.org/10.1029/2018GL080830

Nishimura, T., Matsuzawa, T., & Obara, K. (2013). Detection of short-term slow slip events along the Nankai Trough, southwest Japan, using GNSS data. *Journal of Geophysical Research: Solid Earth*, *118*(6), 3112–3125. https://doi.org/10.1002/jgrb.50222

Ozawa, S. (2014). Shortening of recurrence interval of Boso slow slip events in Japan. *Geophysical Research Letters*, *41*(8), 2762–2768. https://doi.org/10.1002/2014GL060072

Polster, A., Fabian, M., & Villinger, H. (2009). Effective resolution and drift of paroscientific pressure sensors derived from long-term seafloor measurements. *Geochemistry, Geophysics, Geosystems*, *10*(8). https://doi.org/10.1029/2009GC002532

Ponte, R. M., & Ray, R. D. (2002). Atmospheric pressure corrections in geodesy and oceanography: A strategy for handling air tides. *Geophysical Research Letters*, *29*(24), 6-1-6–4. https://doi.org/10.1029/2002gl016340

Ray, R. D. (2013). Precise comparisons of bottom-pressure and altimetric ocean tides. *Journal of Geophysical Research: Oceans*, *118*(9), 4570–4584. https://doi.org/10.1002/jgrc.20336

Sato, T., Hasegawa, S., Kono, A., Shiobara, H., Yagi, T., Yamada, T., et al. (2017). Detection of vertical motion during a slow-slip event off the Boso Peninsula, Japan, by ocean bottom pressure gauges. *Geophysical Research Letters*, *44*(6), 2710–2715. https://doi.org/10.1002/2017GL072838

Suzuki, K., Nakano, M., Takahashi, N., Hori, T., Kamiya, S., Araki, E., et al. (2016). Synchronous changes in the seismicity rate and ocean-bottom hydrostatic pressures along the Nankai trough: A possible slow slip event detected by the Dense Oceanfloor Network system for Earthquakes and Tsunamis (DONET). *Tectonophysics*, *680*, 90–98. https://doi.org/10.1016/j.tecto.2016.05.012

Todd, E. K., Schwartz, S. Y., Mochizuki, K., Wallace, L. M., Sheehan, A. F., Webb, S. C., et al. (2018). Earthquakes and Tremor Linked to Seamount Subduction During Shallow Slow Slip at the Hikurangi Margin, New Zealand. *Journal of Geophysical Research: Solid Earth*, *123*(8), 6769–6783. https://doi.org/10.1029/2018JB016136

Wallace, L., Webb, S., Ito, Y., Mochizuki, K., Hino, R., Henrys, S., et al. (2016). Slow slip near the trench at the Hikurangi subduction zone, New Zealand. *Science*, *352*(6286), 701–704. https://doi.org/10.1126/science.aaf2349

Wallace, L. M., & Beavan, J. (2010). Diverse slow slip behavior at the Hikurangi subduction margin, New Zealand. *Journal of Geophysical Research: Solid Earth*, *115*(12), 1–20. https://doi.org/10.1029/2010JB007717

Warren-Smith, E., Fry, B., Wallace, L., Chon, E., Henrys, S., Sheehan, A., et al. (2019). Episodic stress and fluid pressure cycling in subducting oceanic crust during slow slip. *Nature Geoscience*, *12*(6), 475–481. https://doi.org/10.1038/s41561-019-0367-x

Wessel, P., Smith, W. H. F., Scharroo, R., Luis, J., & Wobbe, F. (2013). Generic mapping tools: Improved version released. *Eos*, *94*(45), 409–410. https://doi.org/10.1002/2013EO450001

Yarce, J., Sheehan, A. F., Nakai, J. S., Schwartz, S. Y., Mochizuki, K., Savage, M. K., et al. (2019). Seismicity at the Northern Hikurangi Margin, New Zealand, and Investigation of the Potential Spatial and Temporal Relationships With a Shallow Slow Slip Event. *Journal of Geophysical Research: Solid Earth*, *124*(5), 4751–4766. https://doi.org/10.1029/2018JB017211

Yohler, R., Bartlow, N., Wallace, L. M., & Williams, C. (2019). Time-Dependent Behavior of a Near-Trench Slow-Slip Event at the Hikurangi Subduction Zone. *Geochemistry, Geophysics, Geosystems*, *20*(8), 4292–4304. https://doi.org/10.1029/2019GC008229

Zal, H. J., Jacobs, K., Savage, M. K., Yarce, J., Mroczek, S., Graham, K., et al. (2020). Temporal and spatial variations in seismic anisotropy and VP/VS ratios in a region of slow slip. *Earth and Planetary Science Letters*, *532*, 115970. https://doi.org/10.1016/j.epsl.2019.115970

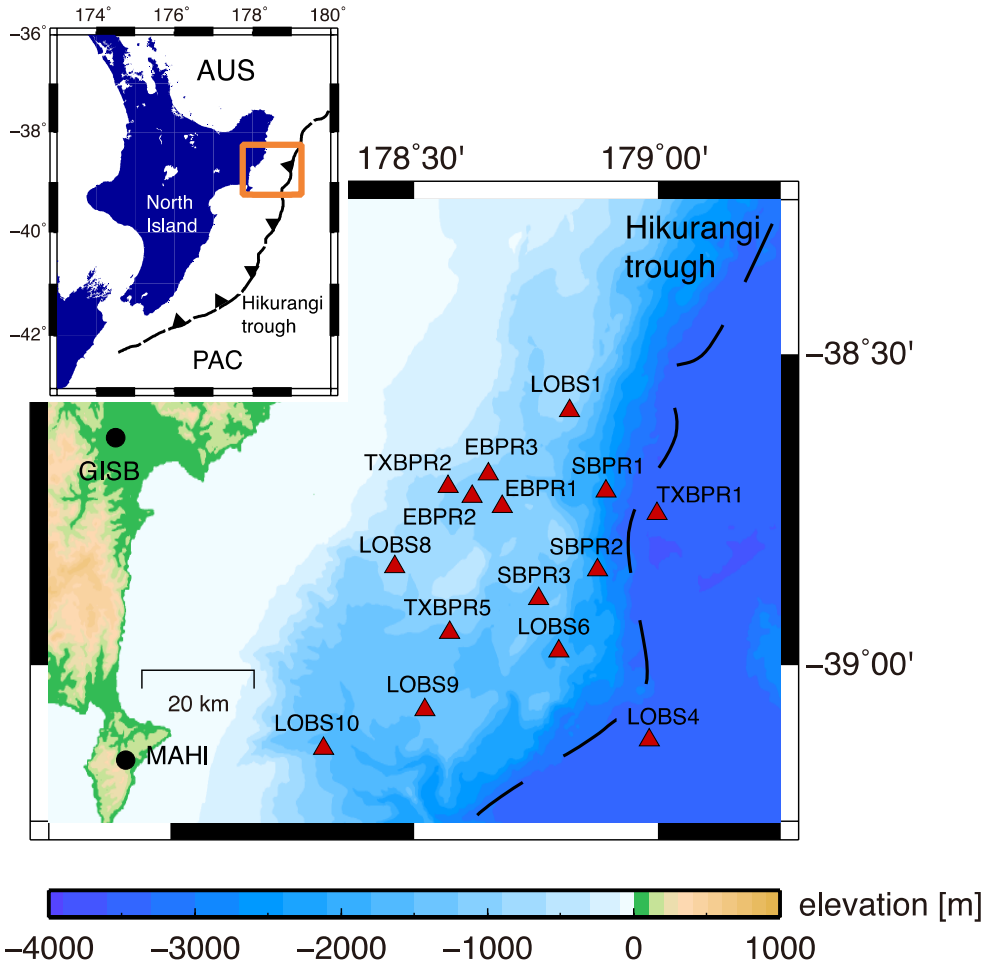

Figure 1. Map of the study area and the network map of the OBP gauges. Triangles and circles indicate stations for OBP and land GNSS sites, respectively. AUS and PAC indicate the Australian and Pacific plates, respectively.

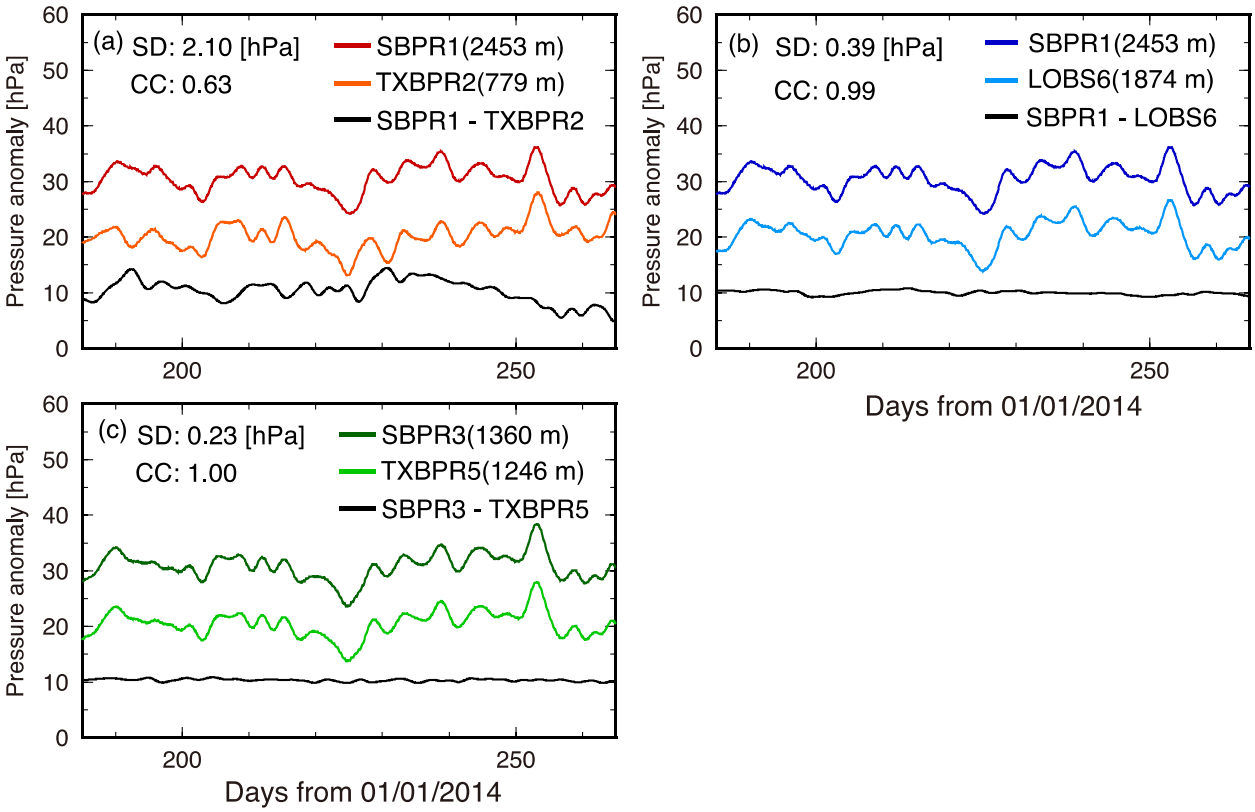

Figure 2. An example of the OBP time series. (a) Site pairs with a large difference in depth (depth difference: 1674 m) and a 28.2 km distance between sites. (b) Site pairs with similar depths (depth difference: 579 m) with a 29.1 km distance between sites. (c) Site pairs with similar depths (depth difference: 114 m) with a 29.1 km distance between sites.

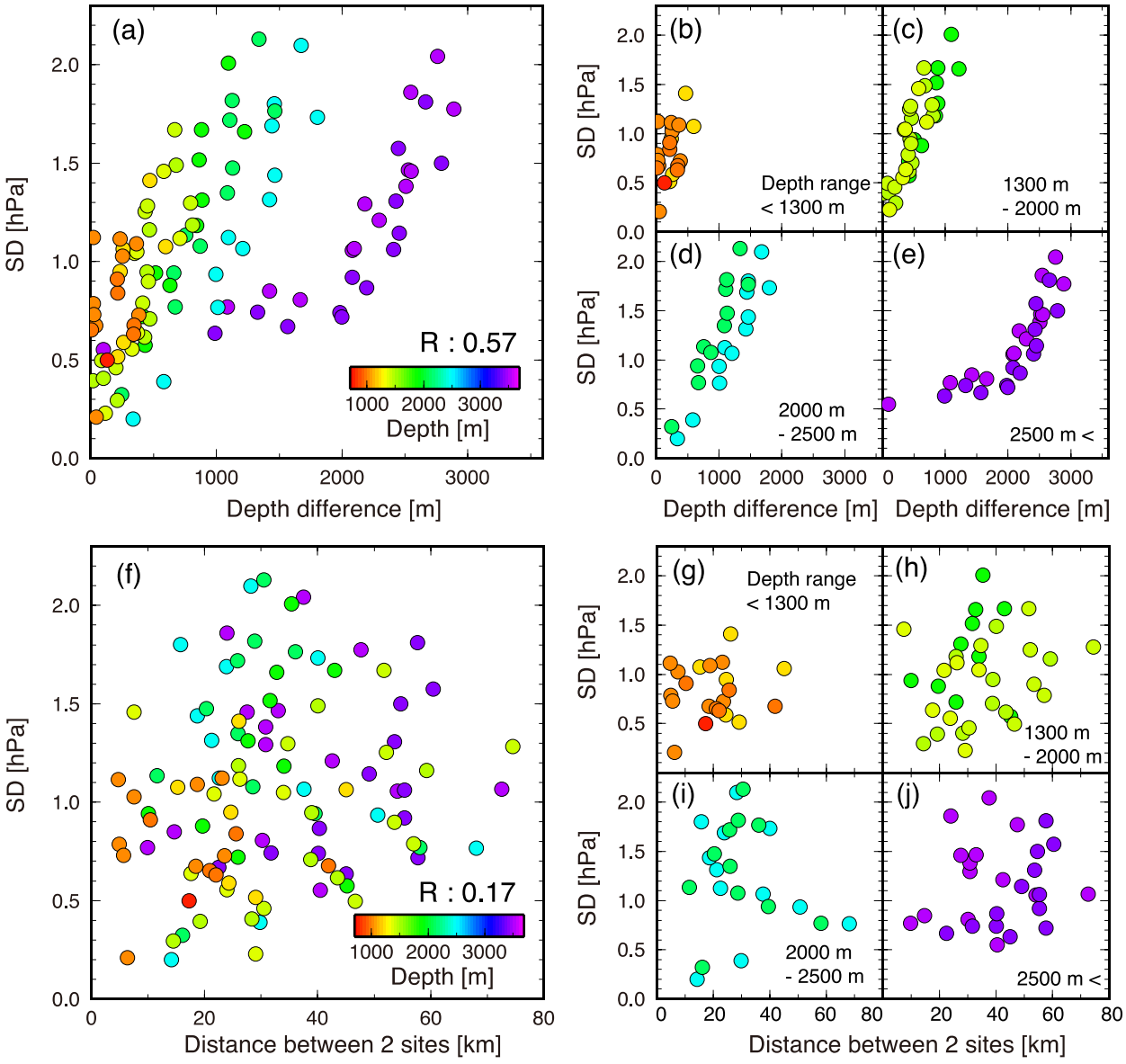

Figure 3. The relationship between the standard deviation (SD) of the residual observed pressure in the period (185–265 days) and the absolute depth difference (a–e) and the distance (f–j) between two sites. Colored circles indicate the depth of the deeper site of each pair of sites (a–j). The R value indicates the correlation coefficient of the distribution between SD and depth difference (a) or the distances between the 2 sites (f). (b–e) and (g–j) are separated into four sets of site depths, using the data from (a) and (f).

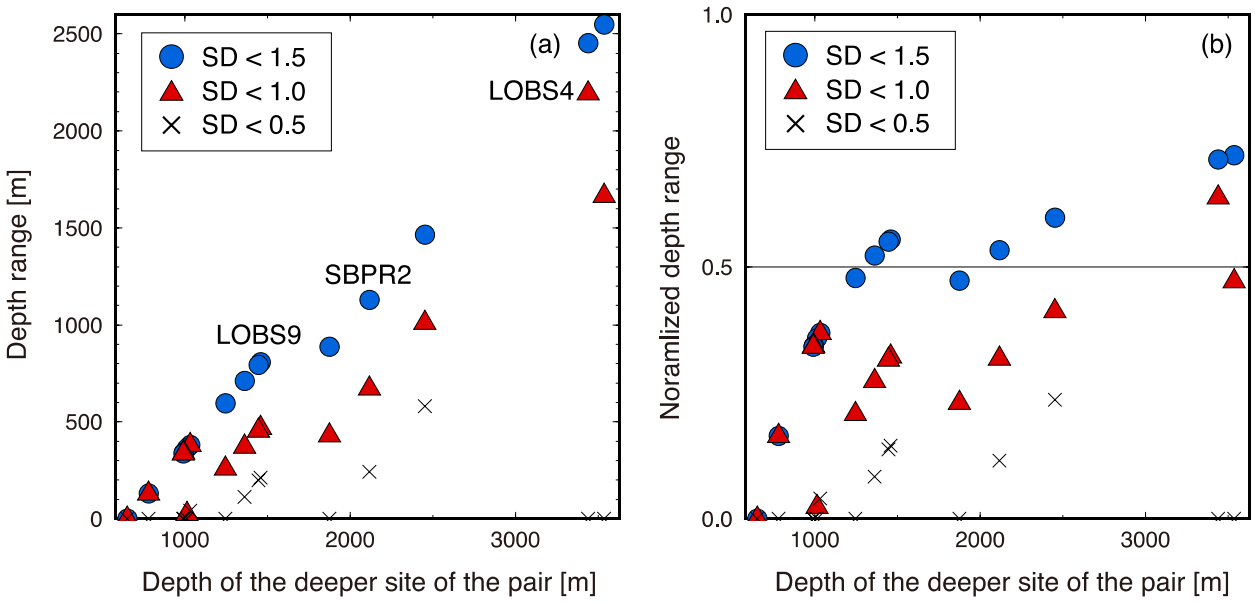

Figure 4. (a) Comparison of the SD (blue circle: < 1.5 hPa, red triangle: < 1.0 hPa, and black cross: < 0.5hPa) thresholds for the depth ranges relative to the depth of the deepest site of the pairs. (b) Comparison of the SDs for normalized depth ranges relative to the depth of the deepest site of the pairs. Normalized depth is calculated by dividing the depth range by each depth of the deepest site of the pairs.